

Received 29 November 2022
Accepted 12 January 2023

Edited by M. Weil, Vienna University of Technology, Austria

This article is part of a collection of articles to commemorate the founding of the African Crystallographic Association and the 75th anniversary of the IUCr.

Keywords: crystal structure; orthophosphates; solid-state reactions; α -CrPO₄-type structure BaNi₂Fe(PO₄)₃.

CCDC reference: 2172184

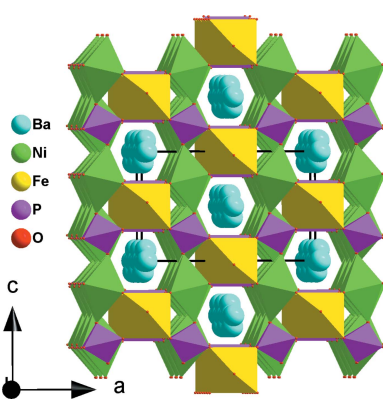
Supporting information: this article has supporting information at journals.iucr.org/e

Crystal structure of barium dinickel(II) iron(III) tris[orthophosphate(V)], BaNi₂Fe(PO₄)₃

Said Ouaatta,^{a*} Adam Bouraima,^{a,b} Elhassan Benhsina,^a Jamal Khmiyas,^a Abderrazzak Assani,^a Mohamed Saadi^a and Lahcen El Ammari^a

^aLaboratoire de Chimie Appliquée des Matériaux, Centre des Sciences des Matériaux, Faculty of Science, Mohammed V University in Rabat, Avenue Ibn Batouta, BP 1014, Rabat, Morocco, and ^bLaboratoire de Chimie des Matériaux Inorganiques, Faculté des Sciences, Département de Chimie, Université des Sciences et Techniques de Masuku, BP 943, Franceville, Gabon. *Correspondence e-mail: saidouatta87@gmail.com

The orthophosphate BaNi₂Fe(PO₄)₃ has been synthesized by a solid-state reaction route and characterized by single-crystal X-ray diffraction and energy-dispersive X-ray spectroscopy. The crystal structure comprises (100) sheets made up of [Ni₂O₁₀] dimers that are linked to two PO₄ tetrahedra via common edges and vertices and of linear infinite [010] chains of corner-sharing [FeO₆] octahedra and [PO₄] tetrahedra. The linkage of the sheets and chains into a framework is accomplished through common vertices of PO₄ tetrahedra and [FeO₆] octahedra. The framework is perforated by channels in which positionally disordered Ba²⁺ cations are located.



OPEN ACCESS

Published under a CC BY 4.0 licence

1. Chemical context

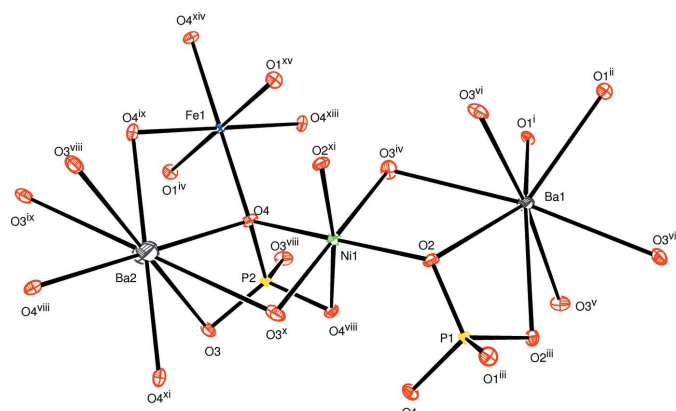
Phosphate-based materials have been studied extensively in the past. Among them are orthophosphates, which have gained great interest in recent years owing to their structural richness (Maeda, 2004) and their promising applications, for example in electrochemical catalysis (Dwibedi *et al.*, 2020; Cheng *et al.*, 2021; Rekha *et al.*, 2021; Anahmadi *et al.*, 2022). Furthermore, orthophosphates doped with rare-earth cations have shown excellent optical properties (Ci *et al.*, 2014; Li *et al.*, 2021; Indumathi *et al.*, 2022), along with a wide range of applications for use in luminescence emission displays (Li *et al.*, 2008; Wan *et al.*, 2010; Yang *et al.*, 2019; Santos *et al.*, 2022).

In this context, our research interest is connected with tris-orthophosphate-based materials with general formula $(A_2/B)M_2M'(\text{PO}_4)_3$, where A can be an alkali, B an alkaline earth and M and M' transition metal cations. The crystal structures of these orthophosphates adopt the α -CrPO₄ type of structure, consisting of a three-dimensional framework made up of [MO₆] and [M'O₆] octahedra sharing corners and/or edges with PO₄ tetrahedra. This framework is permeated by channels in which the A or B cations are located.

We report herein on the synthesis and structural characterization of barium dinickel(II) iron(III) tris-orthophosphate, BaNi₂Fe(PO₄)₃.

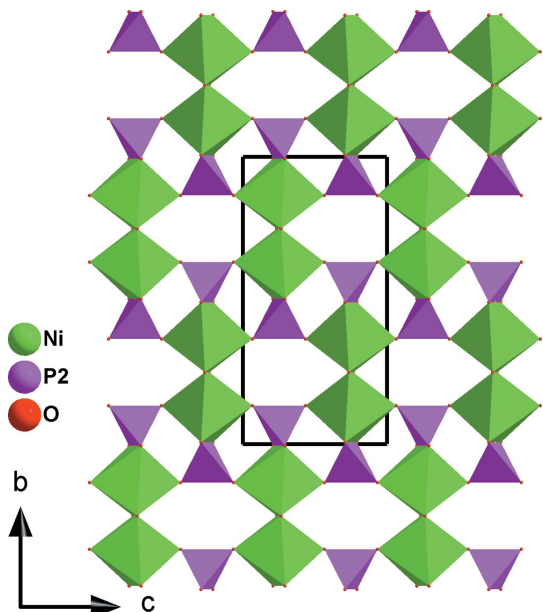
2. Structural commentary

The title compound is related to the strontium and calcium homologs MNi₂Fe(PO₄)₃ ($M = \text{Sr, Ca}$; Ouaatta *et al.*, 2015, 2017), all adopting the α -CrPO₄ structure type (Attfield *et al.*, 1986). The asymmetric unit of BaNi₂Fe(PO₄)₃ is comprised of

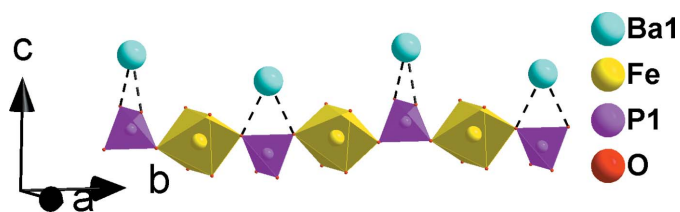
**Figure 1**

The principal building units in the crystal structure of the title compound. Displacement ellipsoids are drawn at the 50% probability level. [Symmetry codes: (i) $-x + 1, -y + \frac{1}{2}, z - 1$; (ii) $x, y, z - 1$; (iii) $-x + 1, -y + \frac{1}{2}, z$; (iv) $-x + \frac{3}{2}, -y + 1, z - \frac{1}{2}$; (v) $x - \frac{1}{2}, y - \frac{1}{2}, z - \frac{1}{2}$; (vi) $-x + \frac{3}{2}, y - \frac{1}{2}, z - \frac{1}{2}$; (vii) $x - \frac{1}{2}, -y + 1, z - \frac{1}{2}$; (viii) $-x + 2, -y + 1, -z + 2$; (ix) $-x + 2, y, z$; (x) $x, -y + 1, -z + 2$; (xi) $-x + \frac{3}{2}, -y + \frac{1}{2}, -z + \frac{3}{2}$; (xii) $-x + \frac{3}{2}, y, -z + \frac{3}{2}$; (xiii) $x, -y + 1, -z + 1$; (xiv) $-x + 2, -y + 1, -z + 1$; (xv) $x + \frac{1}{2}, y, -z + \frac{3}{2}$].

ten sites, eight of which are on special positions, except the O3 and O4 sites on a general position (Wyckoff position 16*j*). Ba1 (site occupation 0.9868) exhibits site symmetry *mm*2 (4*e*), Ba2 (site occupation 0.0132) 2/*m* (4*a*), Fe1 2/*m* (4*b*), Ni1 2 (8*g*), P1 1*m*2 (4*e*), P2 2 (8*g*), while O1 and O2 occupy sites with *m* (8*h*) and *m* (8*i*) symmetry, respectively. The framework structure of $\text{BaNi}_2\text{Fe}(\text{PO}_4)_3$ is composed of extended (100) sheets and linear infinite chains extending parallel to [010] (Fig. 1). The (100) sheets are made up from edge-sharing $[\text{Ni}_2\text{O}_{10}]$ dimers linked to two P_2O_4 tetrahedra via common edges to form an $[\text{Ni}_2\text{P}_2\text{O}_{14}]$ unit that is linked to four neighboring units (Fig. 2). Between these sheets appear the

**Figure 2**

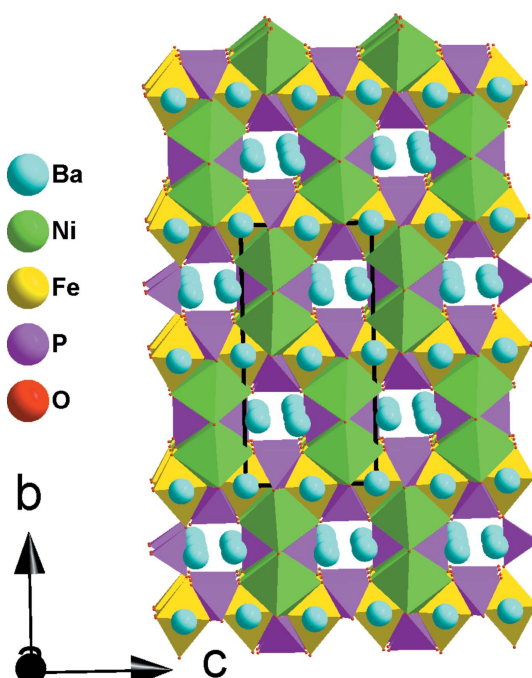
Projection of a (100) sheet along [100] showing the $[\text{Ni}_2\text{P}(2)_2\text{O}_{14}]$ unit.

**Figure 3**

A chain formed by sharing corners of $[\text{FeO}_6]$ octahedra and P_1O_4 tetrahedra, alternating with a zigzag arrangement of barium cations (Ba1) along [010].

linear infinite chains resulting from the alternating linkage of P_1O_4 tetrahedra and $[\text{FeO}_6]$ octahedra, which are surrounded by a zigzag arrangement of Ba^{2+} cations (Fig. 3). The sheets and chains are linked through common vertices of PO_4 tetrahedra and $[\text{FeO}_6]$ octahedra into a framework, which delimits two types of channels parallel to [100] and [010] in which the disordered Ba^{2+} cations are located (Figs. 4, 5).

To confirm the structure model of $\text{BaNi}_2\text{Fe}(\text{PO}_4)_3$, the bond-valence method (Brown, 1977; 1978; Brown & Altermatt, 1985) and charge distribution (CHARDI) concept (Hoppe *et al.*, 1989) were employed by making use of the programs EXPO2014 (Altomare *et al.*, 2013) and CHARDI2015 (Nespolo & Guillot, 2016), respectively. Table 1 compiles all cationic valences $V(i)$ computed with the bond-valence method and their related charges $Q(i)$ obtained with the CHARDI concept. The resulting $Q(i)$ and $V(i)$ values are all close to the corresponding charges $q(i) \times \text{sof}(i)$ [$q(i)$ are formal oxidation numbers weighted by the site occupation

**Figure 4**

Polyhedral representation of the crystal structure of $\text{BaNi}_2\text{Fe}(\text{PO}_4)_3$ showing Ba1 in the channels running along the [100] direction and a row of underoccupied Ba2 along [001].

Table 1

Bond valence and CHARDI analyses for the cations in the title compound.

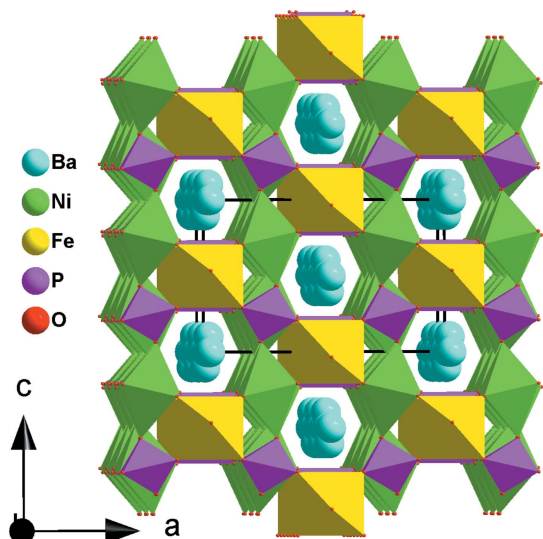
$q(i)$ = formal oxidation number; $\text{sof}(i)$ = site occupancy; $\text{CN}(i)$ = classical coordination number; $Q(i)$ = calculated charge; $V(i)$ = calculated valence; $\text{ECoN}(i)$ = effective coordination number.

Cation	$q(i)$	$\text{sof}(i)$	$\text{CN}(i)$	$\text{ECoN}(i)$	$V(i)$	$Q(i)$	$q(i)/Q(i)$
Ba1	1.98	0.99	8	7.99	2.37	1.98	1.00
Ba2	0.02	0.01	8	5.43	0.02	0.99	
Ni	2.00	1.00	6	5.97	2.00	1.98	1.01
Fe	3.00	1.00	4	5.96	3.01	2.99	1.00
P1	5.00	1.00	4	3.99	4.95	4.83	1.04
P2	5.00	1.00	4	3.96	4.85	5.11	0.98

factors $\text{sof}(i)$]. In summary, the expected oxidation states of Ba^{2+} , Ni^{2+} , Fe^{3+} and P^{5+} are predicted through the charge distribution. The internal criterion $q(i)/Q(i)$ is very near to 1 for all ionic species and the mean absolute percentage deviation (MAPD), which gives a measure for the agreement between the $q(i)$ and $Q(i)$ charges, is just 1.3%, thus confirming the validity of the structure model (Eon & Nespolo, 2015). The global instability index (GII; Salinas-Sánchez *et al.*, 1992) of 0.13 is a further confirmation of the structure model.

3. Database survey

It is reasonable to compare the crystal structure of the title compound with that of $\alpha\text{-CrPO}_4$ (Glaum *et al.*, 1986). Both phosphates crystallize in the orthorhombic system in space group type *Imma*. Their unit-cell parameters are nearly the same despite the differences between their chemical formulae. In the structure of $\alpha\text{-CrPO}_4$, the Cr^{3+} and P^{5+} cations occupy four special positions that are part of a framework comprised of $[\text{CrO}_6]$ octahedra and $[\text{PO}_4]$ tetrahedra. The resultant framework is permeated by vacant channels along

**Figure 5**

Polyhedral representation of the crystal structure of $\text{BaNi}_2\text{Fe}(\text{PO}_4)_3$ showing Ba1 and Ba2 in the channels.

Table 2

Atom percentages in $\text{BaNi}_2\text{Fe}(\text{PO}_4)_3$ as determined by EDS.

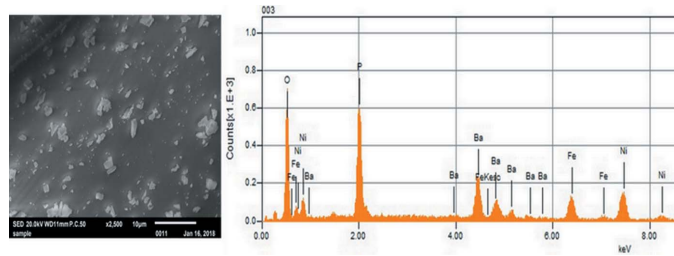
Element	Atomic percentage	Sigma
O	56.74	0.13
P	19.60	0.16
Fe	5.63	0.17
Ni	12.25	0.27
Ba	5.78	0.30
Total	100.00	

[100] and [010]. The formula of $\alpha\text{-CrPO}_4$ can be written as $X1X2\text{Cr}_1\text{Cr}_2(\text{PO}_4)_3$, where $X1$, $X2$ represent the empty channel sites. Accordingly, the substitution of Cr1 or Cr2 by a divalent cation requires charge compensation by cations located in the channels to result in $AA'MM'_2(\text{PO}_4)_3$ compounds such as $\text{BaNi}_2\text{Fe}(\text{PO}_4)_3$, or $M\text{Ni}_2\text{Fe}(\text{PO}_4)_3$ (M = Sr, Ca; Ouaatta *et al.*, 2015, 2017). The difference between $\text{BaNi}_2\text{Fe}(\text{PO}_4)_3$ and the closely related $M\text{Ni}_2\text{Fe}(\text{PO}_4)_3$ structures pertains to the M site, which is split into two sites for the title compound and fully occupied for M = Ca, Sr.

4. Synthesis and crystallization

$\text{BaNi}_2\text{Fe}(\text{PO}_4)_3$ was prepared from a mixture of $\text{Ba}(\text{NO}_3)_2$ (Merck, 98.5%), $\text{Ni}(\text{NO}_3)_2 \cdot 6\text{H}_2\text{O}$ (Riedel-de-Haén, 97%), $\text{Fe}(\text{NO}_3)_3 \cdot 9\text{H}_2\text{O}$ (Panreac, 98%) and H_3PO_4 (85%_{w/w}) in the molar ratio of $\text{Ba:Ni:Fe:P} = 1:2:1:3$. The precursors were suspended in 50 ml of distilled water and stirred without warming for 24 h before heating to dryness at 373 K. The obtained dry residue was ground in an agate mortar until homogeneous, subsequently heated in a platinum crucible up to 673 K to remove volatile decomposition products, and then melted at 1433 K. After being kept at this temperature for one h, the melt was cooled down slowly at a rate of 5 K h⁻¹ to 1233 K and then to room temperature. Single crystals with a brown color and different forms were obtained after leaching with distilled water.

Chemical analysis of the title phosphate was performed with an energy-dispersive X-ray spectroscopy (EDS) microprobe mounted on a JEOL JSM-IT100 in TouchScope™ scanning electron microscope. The EDS spectrum is depicted in Fig. 6 and confirms the presence of only barium, nickel, iron, phosphorus and oxygen in approximately the correct ratios, as shown in Table 2.

**Figure 6**

SEM micrograph and results of an EDS measurement of the title compound.

Table 3
Experimental details.

Crystal data	BaNi ₂ Fe(PO ₄) ₃
Chemical formula	
M_r	595.52
Crystal system, space group	Orthorhombic, <i>Imma</i>
Temperature (K)	296
a, b, c (Å)	10.4711 (2), 13.2007 (3), 6.6132 (1)
V (Å ³)	914.12 (3)
Z	4
Radiation type	Mo $K\alpha$
μ (mm ⁻¹)	10.46
Crystal size (mm)	0.32 × 0.25 × 0.19
Data collection	
Diffractometer	Bruker X8 APEX Diffractometer
Absorption correction	Multi-scan (<i>SADABS</i> ; Krause <i>et al.</i> , 2015)
T_{\min}, T_{\max}	0.624, 0.748
No. of measured, independent and observed [$I > 2\sigma(I)$] reflections	18099, 1460, 1440
R_{int}	0.029
(sin θ/λ) _{max} (Å ⁻¹)	0.893
Refinement	
$R[F^2 > 2\sigma(F^2)], wR(F^2), S$	0.015, 0.036, 1.21
No. of reflections	1460
No. of parameters	58
$\Delta\rho_{\max}, \Delta\rho_{\min}$ (e Å ⁻³)	1.33, -0.78

Computer programs: *APEX3* (Bruker, 2016), *SAINT* (Bruker, 2016), *SAINT* (Bruker, 2016), *SHELXT2014/4* (Sheldrick, 2015a), *SHELXL2018/3* (Sheldrick, 2015b), *ORTEP-3 for Windows* (Farrugia, 2012), *DIAMOND* (Brandenburg, 2006), *publCIF* (Westrip, 2010).

5. Refinement

Crystal data, data collection and structure refinement details are summarized in Table 3. After assignment of the atomic sites according to the related $M\text{Ni}_2\text{Fe}(\text{PO}_4)_3$ structures ($M = \text{Sr, Ca}$; Ouaatta *et al.*, 2015, 2017), a difference-Fourier map revealed a maximum electron density of 3.61 Å⁻³ that was finally modeled as a considerably underoccupied Ba site (Ba2). For the final model, the sum of site-occupation factors for the Ba1 and Ba2 sites were constrained to be 1. The highest remaining maximum and minimum electronic densities are 0.59 Å and 0.47 Å from Ba1 and Ni1, respectively.

Acknowledgements

The authors thank the Faculty of Science, Mohammed V University in Rabat, for the X-ray measurements.

References

- Altomare, A., Cuocci, C., Giacovazzo, C., Moliterni, A., Rizzi, R., Corriero, N. & Falcicchio, A. (2013). *J. Appl. Cryst.* **46**, 1231–1235.
- Anahmadi, H., Fathi, M., El hajri, F., Benzekri, Z., Sibous, S., Idrissi, B. C., El youbi, M. S., Souizi, A. & Boukhris, S. (2022). *J. Mol. Struct.* **1248**, 131449.
- Attfield, J. P., Sleight, A. W. & Cheetham, A. K. (1986). *Nature* **322**, 620–622.
- Brandenburg, K. (2006). *DIAMOND*. Crystal Impact GbR, Bonn, Germany.
- Brown, I. D. (1977). *Acta Cryst.* **B33**, 1305–1310.
- Brown, I. D. (1978). *Chem. Soc. Rev.* **7**, 359–376.
- Brown, I. D. & Altermann, D. (1985). *Acta Cryst.* **B41**, 244–247.
- Bruker, (2016). *APEX3* and *SAINT*. Bruker AXS Inc., Madison, Wisconsin, USA.
- Cheng, Q., Zhao, X., Yang, G., Mao, L., Liao, F., Chen, L., He, P., Pan, D. & Chen, S. (2021). *Energy Storage Materials*, **41**, 842–882.
- Ci, Z., Que, M., Shi, Y., Zhu, G. & Wang, Y. (2014). *Inorg. Chem.* **53**, 2195–2199.
- Dwibedi, D., Barpanda, P. & Yamada, A. (2020). *Small Methods*, **4**, 2000051.
- Eon, J.-G. & Nespolo, M. (2015). *Acta Cryst.* **B71**, 34–47.
- Farrugia, L. J. (2012). *J. Appl. Cryst.* **45**, 849–854.
- Glaum, R., Gruehn, R. & Möller, M. (1986). *Z. Anorg. Allg. Chem.* **543**, 111–116.
- Hoppe, R., Voigt, S., Glaum, H., Kissel, J., Müller, H. P. & Bernet, K. (1989). *J. Less-Common Met.* **156**, 105–122.
- Indumathi, K., Tamilselvan, S., Rajasekaran, L., David, A. D. J., Muhammad, G. S., Ramalingam, G. & Biruntha, M. (2022). *Mater. Lett.* **309**, 131371.
- Krause, L., Herbst-Irmer, R., Sheldrick, G. M. & Stalke, D. (2015). *J. Appl. Cryst.* **48**, 3–10.
- Li, Y. Q., Hirosaki, N., Xie, R. J., Takeda, T. & Mitomo, M. (2008). *Chem. Mater.* **20**, 6704–6714.
- Li, Z., Geng, X., Wang, Y. & Chen, Y. (2021). *J. Lumin.* **240**, 118428.
- Maeda, K. (2004). *Microporous Mesoporous Mater.* **73**, 47–55.
- Nespolo, M. & Guillot, B. (2016). *J. Appl. Cryst.* **49**, 317–321.
- Ouaatta, S., Assani, A., Saadi, M. & El Ammari, L. (2015). *Acta Cryst.* **E71**, 1255–1258.
- Ouaatta, S., Assani, A., Saadi, M. & El Ammari, L. (2017). *Acta Cryst.* **E73**, 893–895.
- Rekha, P., Yadav, S. & Singh, L. (2021). *Ceram. Int.* **47**, 16385–16401.
- Salinas-Sánchez, A., García-Muñoz, J. L., Rodríguez-Carvajal, J., Saez-Puche, R. & Martínez, J. L. (1992). *J. Solid State Chem.* **100**, 201–211.
- Santos, R. D. S., Oliveira, J. L., Araujo, R. M. & Rezende, M. V. dos S. (2022). *J. Solid State Chem.* **306**, 122769.
- Sheldrick, G. M. (2015a). *Acta Cryst.* **A71**, 3–8.
- Sheldrick, G. M. (2015b). *Acta Cryst.* **C71**, 3–8.
- Wan, C., Meng, J., Zhang, F., Deng, X. & Yang, C. (2010). *Solid State Commun.* **150**, 1493–1495.
- Westrip, S. P. (2010). *J. Appl. Cryst.* **43**, 920–925.
- Yang, X., Chen, J., Chai, C., Zheng, S. & Chen, C. (2019). *Optik (Stuttg.)*, **198**, 163238.

supporting information

Acta Cryst. (2023). E79, 95–98 [https://doi.org/10.1107/S2056989023000336]

Crystal structure of barium dinickel(II) iron(III) tris[orthophosphate(V)], $\text{BaNi}_2\text{Fe}(\text{PO}_4)_3$

Said Ouaatta, Adam Bouraima, Elhassan Benhsina, Jamal Khmiyas, Abderrazzak Assani, Mohamed Saadi and Lahcen El Ammari

Computing details

Data collection: *APEX3* (Bruker, 2016); cell refinement: *SAINT* (Bruker, 2016); data reduction: *SAINT* (Bruker, 2016); program(s) used to solve structure: *SHELXT2014/4* (Sheldrick, 2015a); program(s) used to refine structure: *SHELXL2018/3* (Sheldrick, 2015b); molecular graphics: *ORTEP-3 for Windows* (Farrugia, 2012), *DIAMOND* (Brandenburg, 2006); software used to prepare material for publication: *publCIF* (Westrip, 2010).

Barium dinickel(II) iron(III) tris[orthophosphate(V)]

Crystal data

$\text{BaNi}_2\text{Fe}(\text{PO}_4)_3$
 $M_r = 595.52$
Orthorhombic, *Imma*
 $a = 10.4711 (2)$ Å
 $b = 13.2007 (3)$ Å
 $c = 6.6132 (1)$ Å
 $V = 914.12 (3)$ Å³
 $Z = 4$
 $F(000) = 1116$

$D_x = 4.327 \text{ Mg m}^{-3}$
Mo $K\alpha$ radiation, $\lambda = 0.71073$ Å
Cell parameters from 1460 reflections
 $\theta = 3.1\text{--}39.4^\circ$
 $\mu = 10.46 \text{ mm}^{-1}$
 $T = 296 \text{ K}$
Block, colourless
 $0.32 \times 0.25 \times 0.19$ mm

Data collection

Bruker X8 APEX Diffractometer
Radiation source: fine-focus sealed tube
Graphite monochromator
 φ and ω scans
Absorption correction: multi-scan
(SADABS; Krause *et al.*, 2015)
 $T_{\min} = 0.624$, $T_{\max} = 0.748$
18099 measured reflections

1460 independent reflections
1440 reflections with $I > 2\sigma(I)$
 $R_{\text{int}} = 0.029$
 $\theta_{\max} = 39.4^\circ$, $\theta_{\min} = 3.1^\circ$
 $h = -18 \rightarrow 13$
 $k = -23 \rightarrow 23$
 $l = -11 \rightarrow 11$

Refinement

Refinement on F^2
Least-squares matrix: full
 $R[F^2 > 2\sigma(F^2)] = 0.015$
 $wR(F^2) = 0.036$
 $S = 1.21$
1460 reflections
58 parameters
0 restraints

Primary atom site location: structure-invariant direct methods
Secondary atom site location: difference Fourier map
 $w = 1/[\sigma^2(F_o^2) + (0.0147P)^2 + 1.8221P]$
where $P = (F_o^2 + 2F_c^2)/3$
 $(\Delta/\sigma)_{\max} = 0.001$
 $\Delta\rho_{\max} = 1.33 \text{ e } \text{\AA}^{-3}$
 $\Delta\rho_{\min} = -0.78 \text{ e } \text{\AA}^{-3}$

Extinction correction: *SHELXL2018/3*
 (Sheldrick, 2015b),
 $F_c^* = k F_c [1 + 0.001 x F_c^2 \lambda^3 / \sin(2\theta)]^{-1/4}$
 Extinction coefficient: 0.00403 (16)

Special details

Geometry. All esds (except the esd in the dihedral angle between two l.s. planes) are estimated using the full covariance matrix. The cell esds are taken into account individually in the estimation of esds in distances, angles and torsion angles; correlations between esds in cell parameters are only used when they are defined by crystal symmetry. An approximate (isotropic) treatment of cell esds is used for estimating esds involving l.s. planes.

Fractional atomic coordinates and isotropic or equivalent isotropic displacement parameters (\AA^2)

	<i>x</i>	<i>y</i>	<i>z</i>	$U_{\text{iso}}^*/U_{\text{eq}}$	Occ. (<1)
Ba1	0.500000	0.250000	0.39902 (2)	0.00770 (4)	0.9868
Ba2	1.000000	0.500000	1.000000	0.020 (2)	0.0132
Ni1	0.750000	0.36701 (2)	0.750000	0.00501 (4)	
Fe1	1.000000	0.500000	0.500000	0.00337 (5)	
P1	0.500000	0.250000	0.90454 (8)	0.00317 (8)	
P2	0.750000	0.57020 (3)	0.750000	0.00365 (6)	
O1	0.500000	0.34524 (8)	1.03493 (17)	0.00581 (16)	
O2	0.61939 (10)	0.250000	0.76536 (17)	0.00534 (15)	
O3	0.78276 (8)	0.63385 (6)	0.93423 (13)	0.00771 (12)	
O4	0.86254 (7)	0.49395 (6)	0.70839 (12)	0.00574 (11)	

Atomic displacement parameters (\AA^2)

	U^{11}	U^{22}	U^{33}	U^{12}	U^{13}	U^{23}
Ba1	0.00681 (5)	0.01253 (6)	0.00377 (5)	0.000	0.000	0.000
Ba2	0.014 (5)	0.041 (8)	0.006 (4)	0.000	0.000	0.000 (4)
Ni1	0.00498 (7)	0.00383 (7)	0.00621 (8)	0.000	0.00057 (5)	0.000
Fe1	0.00303 (10)	0.00352 (10)	0.00355 (10)	0.000	0.000	0.00008 (8)
P1	0.00348 (18)	0.00281 (17)	0.00322 (18)	0.000	0.000	0.000
P2	0.00380 (13)	0.00392 (13)	0.00324 (12)	0.000	0.00055 (10)	0.000
O1	0.0078 (4)	0.0033 (3)	0.0063 (4)	0.000	0.000	-0.0014 (3)
O2	0.0042 (4)	0.0063 (4)	0.0055 (4)	0.000	0.0016 (3)	0.000
O3	0.0096 (3)	0.0080 (3)	0.0055 (3)	-0.0024 (2)	0.0007 (2)	-0.0023 (2)
O4	0.0045 (3)	0.0058 (3)	0.0070 (3)	0.0009 (2)	0.0016 (2)	0.0006 (2)

Geometric parameters (\AA , $^\circ$)

Ba1—O1 ⁱ	2.7163 (11)	Ni1—O4	2.0670 (8)
Ba1—O1 ⁱⁱ	2.7163 (11)	Ni1—O4 ^{xii}	2.0670 (8)
Ba1—O2 ⁱⁱⁱ	2.7262 (11)	Ni1—O3 ^x	2.1163 (8)
Ba1—O2	2.7262 (11)	Ni1—O3 ^{iv}	2.1163 (8)
Ba1—O3 ^{iv}	2.7530 (8)	Fe1—O4	1.9944 (8)
Ba1—O3 ^v	2.7530 (8)	Fe1—O4 ^{ix}	1.9944 (8)
Ba1—O3 ^{vi}	2.7530 (8)	Fe1—O4 ^{xiii}	1.9944 (8)
Ba1—O3 ^{vii}	2.7530 (8)	Fe1—O4 ^{xiv}	1.9944 (8)

Ba2—O4	2.4077 (8)	Fe1—O1 ^{iv}	2.0559 (11)
Ba2—O4 ^{viii}	2.4078 (8)	Fe1—O1 ^{xv}	2.0559 (11)
Ba2—O4 ^{ix}	2.4078 (8)	P1—O1	1.5246 (11)
Ba2—O4 ^x	2.4078 (8)	P1—O1 ⁱⁱⁱ	1.5246 (11)
Ba2—O3 ^{ix}	2.9129 (9)	P1—O2	1.5524 (11)
Ba2—O3 ^x	2.9129 (9)	P1—O2 ⁱⁱⁱ	1.5524 (11)
Ba2—O3 ^{viii}	2.9129 (9)	P2—O3	1.5192 (8)
Ba2—O3	2.9129 (9)	P2—O3 ^{xii}	1.5193 (8)
Ni1—O2 ^{xi}	2.0655 (7)	P2—O4 ^{xii}	1.5739 (8)
Ni1—O2	2.0655 (7)	P2—O4	1.5739 (8)
O1 ⁱ —Ba1—O1 ⁱⁱ	55.14 (4)	O4 ^{viii} —Ba2—O3	124.49 (2)
O1 ⁱ —Ba1—O2 ⁱⁱⁱ	141.97 (2)	O4 ^{ix} —Ba2—O3	111.55 (2)
O1 ⁱⁱ —Ba1—O2 ⁱⁱⁱ	141.97 (2)	O4 ^x —Ba2—O3	68.45 (2)
O1 ⁱ —Ba1—O2	141.97 (2)	O3 ^{ix} —Ba2—O3	102.68 (3)
O1 ⁱⁱ —Ba1—O2	141.97 (2)	O3 ^x —Ba2—O3	77.32 (3)
O2 ⁱⁱⁱ —Ba1—O2	54.59 (5)	O3 ^{viii} —Ba2—O3	180.0
O1 ⁱ —Ba1—O3 ^{iv}	109.44 (2)	O2 ^{xi} —Ni1—O2	83.20 (5)
O1 ⁱⁱ —Ba1—O3 ^{iv}	79.47 (2)	O2 ^{xi} —Ni1—O4	102.84 (3)
O2 ⁱⁱⁱ —Ba1—O3 ^{iv}	107.68 (3)	O2—Ni1—O4	172.00 (3)
O2—Ba1—O3 ^{iv}	63.00 (2)	O2 ^{xi} —Ni1—O4 ^{xii}	172.00 (4)
O1 ⁱ —Ba1—O3 ^v	79.47 (2)	O2—Ni1—O4 ^{xii}	102.84 (3)
O1 ⁱⁱ —Ba1—O3 ^v	109.44 (2)	O4—Ni1—O4 ^{xii}	71.66 (4)
O2 ⁱⁱⁱ —Ba1—O3 ^v	63.00 (2)	O2 ^{xi} —Ni1—O3 ^x	86.40 (4)
O2—Ba1—O3 ^v	107.68 (3)	O2—Ni1—O3 ^x	93.14 (4)
O3 ^{iv} —Ba1—O3 ^v	170.30 (4)	O4—Ni1—O3 ^x	92.48 (3)
O1 ⁱ —Ba1—O3 ^{vi}	79.47 (2)	O4 ^{xii} —Ni1—O3 ^x	88.02 (3)
O1 ⁱⁱ —Ba1—O3 ^{vi}	109.44 (2)	O2 ^{xi} —Ni1—O3 ^{iv}	93.14 (4)
O2 ⁱⁱⁱ —Ba1—O3 ^{vi}	107.68 (3)	O2—Ni1—O3 ^{iv}	86.40 (4)
O2—Ba1—O3 ^{vi}	63.00 (2)	O4—Ni1—O3 ^{iv}	88.02 (3)
O3 ^{iv} —Ba1—O3 ^{vi}	67.69 (4)	O4 ^{xii} —Ni1—O3 ^{iv}	92.48 (3)
O3 ^v —Ba1—O3 ^{vi}	111.43 (4)	O3 ^x —Ni1—O3 ^{iv}	179.39 (5)
O1 ⁱ —Ba1—O3 ^{vii}	109.44 (2)	O2 ^{xi} —Ni1—P2	138.40 (2)
O1 ⁱⁱ —Ba1—O3 ^{vii}	79.47 (2)	O2—Ni1—P2	138.40 (2)
O2 ⁱⁱⁱ —Ba1—O3 ^{vii}	63.00 (2)	O4—Fe1—O4 ^{ix}	92.40 (5)
O2—Ba1—O3 ^{vii}	107.68 (3)	O4—Fe1—O4 ^{xiii}	87.60 (5)
O3 ^{iv} —Ba1—O3 ^{vii}	111.43 (4)	O4 ^{ix} —Fe1—O4 ^{xiii}	180.0
O3 ^v —Ba1—O3 ^{vii}	67.69 (4)	O4—Fe1—O4 ^{xiv}	180.0
O3 ^{vi} —Ba1—O3 ^{vii}	170.30 (4)	O4 ^{ix} —Fe1—O4 ^{xiv}	87.60 (5)
O4—Ba2—O4 ^{viii}	180.0	O4 ^{xiii} —Fe1—O4 ^{xiv}	92.40 (5)
O4—Ba2—O4 ^{ix}	73.43 (4)	O4—Fe1—O1 ^{iv}	87.83 (3)
O4 ^{viii} —Ba2—O4 ^{ix}	106.57 (4)	O4 ^{ix} —Fe1—O1 ^{iv}	87.83 (3)
O4—Ba2—O4 ^x	106.57 (4)	O4 ^{xiii} —Fe1—O1 ^{iv}	92.17 (3)
O4 ^{viii} —Ba2—O4 ^x	73.43 (4)	O4 ^{xiv} —Fe1—O1 ^{iv}	92.17 (3)
O4 ^{ix} —Ba2—O4 ^x	180.0	O4—Fe1—O1 ^{xv}	92.17 (3)
O4—Ba2—O3 ^{ix}	111.55 (2)	O4 ^{ix} —Fe1—O1 ^{xv}	92.17 (3)
O4 ^{viii} —Ba2—O3 ^{ix}	68.45 (2)	O4 ^{xiii} —Fe1—O1 ^{xv}	87.83 (3)
O4 ^{ix} —Ba2—O3 ^{ix}	55.51 (2)	O4 ^{xiv} —Fe1—O1 ^{xv}	87.83 (3)

O4 ^x —Ba2—O3 ^{ix}	124.49 (2)	O1 ^{iv} —Fe1—O1 ^{xv}	180.0
O4—Ba2—O3 ^x	68.45 (2)	O1—P1—O1 ⁱⁱⁱ	111.11 (9)
O4 ^{viii} —Ba2—O3 ^x	111.55 (2)	O1—P1—O2	109.59 (3)
O4 ^{ix} —Ba2—O3 ^x	124.49 (2)	O1 ⁱⁱⁱ —P1—O2	109.59 (3)
O4 ^x —Ba2—O3 ^x	55.51 (2)	O1—P1—O2 ⁱⁱⁱ	109.59 (3)
O3 ^{ix} —Ba2—O3 ^x	180.0	O1 ⁱⁱⁱ —P1—O2 ⁱⁱⁱ	109.59 (3)
O4—Ba2—O3 ^{viii}	124.49 (2)	O2—P1—O2 ⁱⁱⁱ	107.28 (9)
O4 ^{viii} —Ba2—O3 ^{viii}	55.51 (2)	O3—P2—O3 ^{xii}	112.84 (7)
O4 ^{ix} —Ba2—O3 ^{viii}	68.45 (2)	O3—P2—O4 ^{xii}	112.49 (4)
O4 ^x —Ba2—O3 ^{viii}	111.55 (2)	O3 ^{xii} —P2—O4 ^{xii}	108.95 (5)
O3 ^{ix} —Ba2—O3 ^{viii}	77.32 (3)	O3—P2—O4	108.95 (5)
O3 ^x —Ba2—O3 ^{viii}	102.68 (3)	O3 ^{xii} —P2—O4	112.49 (4)
O4—Ba2—O3	55.51 (2)	O4 ^{xii} —P2—O4	100.50 (6)

Symmetry codes: (i) $-x+1, -y+1/2, z-1$; (ii) $x, y, z-1$; (iii) $-x+1, -y+1/2, z$; (iv) $-x+3/2, -y+1, z-1/2$; (v) $x-1/2, y-1/2, z-1/2$; (vi) $-x+3/2, y-1/2, z-1/2$; (vii) $x-1/2, -y+1, z-1/2$; (viii) $-x+2, -y+1, -z+2$; (ix) $-x+2, y, z$; (x) $x, -y+1, -z+2$; (xi) $-x+3/2, -y+1/2, -z+3/2$; (xii) $-x+3/2, y, -z+3/2$; (xiii) $x, -y+1, -z+1$; (xiv) $-x+2, -y+1, -z+1$; (xv) $x+1/2, y, -z+3/2$.